# Efficient and Robust Cluster Identification for Ultra-Wideband Propagations Inspired by Biological Ant Colony Clustering

Bin Li, Chenglin Zhao, Haijun Zhang, Zheng Zhou, *Member, IEEE*, and Arumugam Nallanathan, *Senior Member, IEEE*

***Abstract*—Cluster identification of ultra-wideband (UWB) propagations is of great significance to the parameter extraction and measurement analysis of channel modeling. In this paper, we address this challenging problem within a promising biological processing framework. Both the two large-scale characteristics of each multipath component, i.e., the decaying amplitude and the time of arrivals, are organically combined and fully explored in the suggested cluster identification algorithm. Each resolvable trajectory component is first projected onto a 2-D amplitude–time plane and further modeled as a virtual ant-agent, which can move around in this 2-D workspace with a preference to the high local-environment similarity. By establishing a subtle population similarity and specifying an efficient position adaptation strategy, cluster identifications can be realized by the biological ant colony clustering procedure. Owing to the population-based intelligence and the involved positive-feedback collaboration during the agents evolution, the suggested algorithm can efficiently identify the involved multiple clusters in a completely automatic manner. Experiments on UWB channels validate the proposed method. The practical parameter configuration is analyzed, and a group of numerical performance metrics is derived. As demonstrated by numerical investigations, multiple clusters involved in UWB channel impulse responses can be accurately extracted.**

***Index Terms*—Ultra-wideband propagations, cluster identification, ant colony clustering, population similarity.**

## I. Introduction

PROVIDING a fair criterion for performance evaluations of various transmission schemes, channel modeling is always of great importance to the comparative design of physical (PHY) and media access control (MAC) schemes [1]. Owing to the enormous bandwidth ($>$ 500 MHz) of ultra-wideband (UWB) signals and typical short-range application scenarios [2], UWB channel propagations are known to be highly dispersive into hundreds of resolvable multipath components (MPCs) [3]–[5]. This is mainly attributed to the excellent temporal resolution of UWB signals as well as the rich scatters (or reflections) involved in operation environments [2], [6], [7]. The resolvable trajectories, which are reflected from different large objects (e.g., walls and desks), usually arrive in a discontinuous manner, i.e., grouped into several distinguishing *clusters* [5]. This tendency was originally reported by the well-known Saleh-Valenzuela (S-V) indoor channel model [8].

The popular UWB channel modeling, currently favored by the IEEE 802.15.3a wireless personal networks (WPANs) and 802.15.4a wireless sensor networks (WSNs) task groups (TGs), is essentially based on a modified S-V model [9], [10]. In order to further bring these contributions into full play in promoting practical designs, nevertheless, there are still two works to be deepened. First, more experimental measurements of realistic operation environments are required to enrich the parameters database and, therefore, to cover more general UWB applications [4]. It is encouraging to see that, since the birth of first literature on UWB propagations, many works on UWB channel measurements have being reported [11]–[13]. Second, in order to analyze the more detailed structures of UWB channel impulse responses (CIRs), more efficient parameter extraction algorithms may still be desired [11]. Unfortunately, some analysis methods on measured data are relatively elementary and, sometime, may even produce inaccurate results, which may greatly hinder us from drawing more profound conclusions on realistic UWB propagations.

Among these, cluster identification has long remained as a challenging task in the measurement analysis and UWB channel modeling, which is yet of immense significance to propagation characterizations and system designs. First, accurate cluster extraction is the basis for S-V channel modeling [4], [8], [11], [14]. Second, cluster properties can be properly exploited by receiving algorithms, for example in channel estimations [15] and noncoherent detections [16]. Most works in literatures, however, still identify clusters through a time consuming "visual inspection" technique. Such methods generally rely on the subjective assessment from analysts, which on one hand is considerably vulnerable to inconsistency of various observers and, on the other hand, will become impractical for a large amount of measurement data. Reference [17] firstly studied the automatic cluster identification issue by setting up a quantitative criterion of cluster, which may unfortunately produce fake clusters due to serious small-scale fading or

Manuscript received January 6, 2014; revised April 29, 2014, August 7, 2014, and October 16, 2014; accepted November 20, 2014. Date of publication December 4, 2014; date of current version January 14, 2015. This work was supported in part by the National Natural Science Foundation of China under Grant 61471061 and by the Fundamental Research Funds for the Central Universities under Grant 2014RC0101. The editor coordinating the review of this paper and approving it for publication was C. Abou-Rjeily.

B. Li, C. Zhao, and Z. Zhou are with the School of Information and Communication Engineering, Beijing University of Posts and Telecommunications, Beijing 100876, China (e-mail: stonebupt@gmail.com; zz@bupt.edu.cn).

H. Zhang is with the Department of Information Engineering, Beijing University of Chemical Technology, Beijing 100029, China (e-mail: haijun.zhang@kcl.ac.uk).

A. Nallanathan is with the Department of Informatics, King's College London, London WC2R 2LS, U.K. (e-mail: nallanathan@ieee.org).

Color versions of one or more of the figures in this paper are available online at http://ieeexplore.ieee.org.

Digital Object Identifier 10.1109/TCOMM.2014.2377120

specula reflections. Next, by assuming that different clusters with an exponential power delay profile (PDP) may introduce remarkable amplitude discontinuity, [18] suggested a piecewise linear-regression (LR) technique to extract multiple clusters involved in UWB CIRs, and thereby develops a computer-aided cluster identification method. Nevertheless, this mathematically *trial* fitting technique consumes much computation resource [18], [19] and, simultaneously, requires the aid from analysts to develop a reasonable result, making it impractical for large numbers of automatic data processing. More importantly, for more complicated *soft-onset* PDPs [11], this scheme may even become invalid due to the unconscious exponential decay of measured CIRs.

Recently, relying on the conception of discontinuity detections, a new cluster identification scheme is developed [20]. A moving average ratio (MAR) is firstly constructed to reflect amplitude discontinuities aroused by the large-scale fading effect. Such discontinuities are further interpreted as the inter-cluster break points. Then, by resorting to the multi-resolution analysis ability, wavelet transform is used to identify these break points. Finally, multiple clusters are extracted by setting a threshold on wavelet coefficients of the MRA signal. Although this method may produce relatively convincing results, there are still some practical difficulties. Firstly, the thresholding operation suitable for a vehicle cabin is still too simple and, to some extent, even heuristic, which may become invalid to other specific scenarios. Second, the moving average length and wavelet scales should be configured properly as they have significant impacts on identification results. However, the parameters setting can only rely on some empirical researches. Third, the average length is supposed to be large enough to sufficiently suppress the small-scale fading while also small enough to resolve two adjacent clusters. Unfortunately, when the analyzed bandwidth is relatively small or the number of intra-cluster MPCs is few, then confused cluster extractions may be observed, e.g., two adjacent clusters may be interpreted as a single one [20], or false clusters may be generated due to the inefficient suppression of small-scale fading effects. Thus, this algorithm is applicable to some limited circumstances only with the extremely large bandwidth or containing rich intra-cluster MPCs.

Motivated by the considerations above, we develop a new efficient cluster identification scheme inspired by a promising biological ant colony clustering (ACC) mechanic. Firstly, we represent each resolvable MPC as a *virtual* ant-agent, which is projected onto a two-dimensional (2-D) amplitude-time plane. By taking both the decaying amplitudes and time of arrivals (ToAs) into accounts, a subtle environment similarity between neighborhood agents (or multipaths) is designed. Thus, these virtual ants can move around in this 2-D workspace, with a preference to a relatively higher population similarity. Essentially, the similarity metric can be considered as the *likelihood* of MPCs belonging to one cluster. A high environment similarity, therefore, evidences the current neighbor agents sharing more similar properties of decaying amplitudes and ToAs, also suggesting a high probability of intra-cluster MPCs. By exploring the appealing self-adaptation and the underlying positive feedback reinforcement of ACC, the virtual agents with significant similarities and affiliated probably with one unique cluster will be put together into one group finally. In sharp contrast to other classical clustering techniques (such as *K-means*), even without *a priori* clusters number, multiple different clusters can be identified in a completely automatic fashion. Experiments on simulated CIRs validate this proposed scheme, and the extracted clusters keep basically in line with the results of visual inspections. The practical parameters configuration is analyzed and a group of performance metrics are derived numerically. It is demonstrated that the presented algorithm can identify multiple clusters accurately, which may significantly facilitate the parameter extractions in practical channel modeling and, furthermore, deepen our understanding on UWB propagations. This presented method may also provide insights to other time-series analysis (e.g., the analysis of network traffic abnormity).

The rest of the paper is structured as follows. In Section II, the modified S-V channel modeling for UWB, regulated by IEEE 802.15.4a TGs, is described briefly. Subsequently, a new efficient cluster identification algorithm inspired by a biological ant clustering mechanic is developed in Section III. In Section IV, by using UWB CIRs of different scenarios, the practical parameters configuration is discussed. Numerical experiments and performance evaluations of the suggested cluster identification algorithm are also presented. Finally, we conclude the whole investigation in Section V.

## II. UWB Channel Model

### A. Channel Modeling

Owing to the fine temporal resolution of transmitted signals and rich scatters in typical operation environments, the short-range UWB channel is known to be linearly dispersive with tens or hundreds of resolved MPCs [3], [4]. Based on the modified S-V channel modeling, the IEEE 802.15.3a and IEEE 802.15.4a TGs have defined several channel types for UWB applications in dense multipath environments [10]. The unified time domain expression of UWB CIRs can be expressed as

$$h(t) = \chi \sum_{l=0}^{L-1} \sum_{k=0}^{K_l-1} \alpha_{k,l}\delta(t - T_l - \tau_{k,l}), \tag{1}$$

where $L$ is the number of clusters, $K_l$ is the number of rays of the $l$th cluster, $\alpha_{k,l}$ is the fading coefficient of the $k$th path of the $l$th cluster, $\chi$ is the channel shadowing factor. $\alpha_{k,l}$ and $\chi$ are log-normal random variables [3], [4], [9], [10]. $T_l$ is the ToA of the $l$th cluster and $\tau_{k,l}$ is the delay of the $k$th path of the $l$th cluster relative to $T_l$. As suggested, $T_l$ has a Poisson distribution, i.e.,

$$P(T_l|T_{l-1}) = \Upsilon exp\left[-\Upsilon(T_l - T_{l-1})\right],\ l > 0,$$

where $\Upsilon$ is the cluster arrival rate. $\tau_{k,l}$ follow a mixture Poisson distribution, i.e.,

$$P\left(\tau_{k,l}|\tau_{(k-1),l}\right) = \beta\lambda_1 exp\left[-\lambda_1\left(\tau_{k,l} - \tau_{(k-1),l}\right)\right] + (1-\beta)\lambda_2 exp\left[-\lambda_2\left(\tau_{k,l} - \tau_{(k-1),l}\right)\right],\ k > 0, \tag{2}$$

where $\beta$ is the mixture probability; $\lambda_1$ and $\lambda_2$ account for the ray arrival rates of two Poisson processes, respectively [5].

TABLE I
PARAMETERS FOR IEEE 802.15.4A CM1–CM8 MODELS

| CIRs | Environments | LOS/NLOS | Distance $d$ | $\Upsilon$ |
|---|---|---|---|---|
| CM1 | Residential | LOS | 7-20 m | 0.047 [1/ns] |
| CM2 | Residential | NLOS | 7-20 m | 0.12 [1/ns] |
| CM3 | Office | LOS | 3-28 m | 0.16 [1/ns] |
| CM4 | Office | NLOS | 3-28 m | 0.19 [1/ns] |
| CM5 | Outdoor | LOS | 5-17 m | 0.048 [1/ns] |
| CM6 | Outdoor | NLOS | 5-17 m | 0.0243 [1/ns] |
| CM7 | Industrial | LOS | 2-8 m | 0.0709 [1/ns] |
| CM8 | Industrial | NLOS | 2-8 m | 0.09 [1/ns] |

After the small-scale fading has been suppressed, the PDP can be well approximated by the product of two negative exponential functions [3].

$$E\left[|\alpha_{k,l}|^2\right] \propto exp(-T_l/\Gamma)exp(-\tau_{k,l}/\gamma), \quad (3)$$

where $\Gamma$ and $\gamma$ denote the *inter-cluster* and *intra-cluster* decay constants, respectively [4], [10]. Many measurements reveal that the PDP shape may not be always monotonic, but also exhibit a *soft-onset* shape in extreme NLOS situations [4], [10]. In practice, the PDP will increase until a local maximum and then shows decease. The following PDP is suggested to depict the observed phenomenon, i.e.,

$$E\left[|\alpha_{k,l}|^2\right] \propto \left[1-\kappa exp(-\tau_{k,l}/\gamma_{rise})\right] exp(-\tau_{k,l}/\gamma_1), \quad (4)$$

where $\kappa$ denotes the attenuation of the first component, $\gamma_{rise}$ determines how fast the PDP rises to its local maximum, and $\gamma_1$ represents the decay rate at later times [10].

### B. IEEE 802.15.4a Channel Models

The statistical channel model regulated by IEEE 802.15.4a TGs has been widely recommended for evaluating different solutions, which is considered as the most universal model irrespective of the data rate and modulation formats. Such a parametric model is derived from a huge number of realistic measurements [10]. This general model also covers most wireless applications. Typical operating scenarios and corresponding cluster arrival rates of CM1–CM8 are listed in Table I. Such promising applications of UWB are essentially excited by its unique advantages, including the low power consumption, excellent ranging and geolocation capability, etc.

It is suggested that, in order to enrich the parameters database and further reveal some new properties of realistic UWB propagations [3], [4], intensive experimental works are still beneficial. For example, another UWB channel measurement campaign in the frequency-domain has been launched recently [20]–[22] and, after the post-processing on real data [24], a new parametric PDP function, which stems from the Fresh-reflection theory, has been reported [22].

## III. ANT INTELLIGENCE INSPIRED CLUSTER IDENTIFICATION

It has been widely recognized that clusters are groups of MPCs exhibiting the similar larger-scale properties, such as ToAs, angle of arrivals (AoAs) and decaying amplitudes [11], [17], [20], [22]. In other word, the MPCs showing very similar large-scale fading properties (or reflected from the same large object) should be grouped into one cluster, while those exhibiting quite different amplitudes or ToAs characteristics should be put into another cluster. From this point of view, the identification process of multiple clusters can be essentially regarded as a special *data clustering* problem. Due to complicated wireless UWB propagations, unfortunately, such a cluster identification problem may be always beyond the capability of traditional methods.

As is witnessed, on the other hand, most recent researches have been shifted gradually to use biologically-inspired algorithms to perform the complex data processing [25]. Inspired by social insects' behaviors of the real ant (e.g., foraging, nest building, garbage cleaning and territory guarding) [26], [27], ant colony optimization can realize data-clustering by essentially exploiting the population self-similarity, which seems to be in high conjunction with the cluster identification problem in hand. It is noted that, nevertheless, classical ACC methods with unsuitable similarities and random movement strategies may become unattractive to this specific application. In this section, a promising ACC with a new environment similarity and position update rule is specially designed. On this basis, UWB cluster identifications are properly addressed within a promising biological data processing framework by resorting to the ant colony intelligence.

### A. Problem Formulation

In classical ACC methods, e.g., the Lumer and Faieta (LF) algorithm [28], the data object is projected onto a virtual workspace. Then, a population of ant-agents are employed which *randomly* carry (or drop) these data objects with a preference to the low (or high) local environment similarity. With such a formulation, unfortunately, a large amount of ants' aimless (or random) movements may remarkably consume computation resources, leading to the slow convergence in practice [29].

In this investigation, we will adopt another more efficient data clustering formulation. Firstly, each MPC is directly modeled as a *virtual* ant-agent $\boldsymbol{O}_i$, and then projected onto a 2-D *amplitude-time* plane $(x,y)$ which is also referred as to a virtual workspace [29], [30]. Correspondingly, $\boldsymbol{O}_i^{(k)} = [x_i^{(k)}, y_i^{(k)}]$ denotes the position of the $i$th agent during the $k$th iteration. Instead of adopting the classical ant pheromone, we introduce a novel environment similarity $\Lambda_r\left(\boldsymbol{O}_i^{(k)}, \boldsymbol{O}_j^{(k)}\right)$ to describe the local-region fitness (or suitability) which will efficiently guide agents' movements then. The virtual local environment of the $i$th agent $\boldsymbol{O}_i^{(k)}$, denoted by $L\left(\boldsymbol{O}_i^{(k)}, r\right)$, is specified by its sensing range $r$ and the neighbor agents $\boldsymbol{O}_j^{(k)}$ satisfying $\left|\boldsymbol{O}_i^{(k)} - \boldsymbol{O}_j^{(k)}\right| \le r$ [29]. Here, $r$ specifies the largest radius distance between the current agent $\boldsymbol{O}_i^{(k)}$ and its neighbors of interest. During each iteration, the $i$th agent $\boldsymbol{O}_i^{(k)}$ will firstly evaluate its local environment similarity $\Lambda_r\left(\boldsymbol{O}_i^{(k)}, \boldsymbol{O}_j^{(k)}\right)$, and then, decide which

region should move into. Specifically, if the local similarity is very weak (i.e., the current neighbors exhibit quite different properties), then the agent $\boldsymbol{O}_i^{(k)}$ will turn to sense the other feasible region. If the similarity value is significant, indicating the current neighbor agents possibly sharing the unique large-scale effects, it will move close to this region and update its position by $\boldsymbol{O}_i^{(k+1)} = f\left(\boldsymbol{O}_i^{(k)}\right)$, where $f\left(\boldsymbol{O}_i^{(k)}\right)$ accounts for the position update function from the $k$th iteration to the $(k+1)$th iteration.

Relying on the formulation above, the success of this new ant intelligence-based automatic cluster extraction algorithm may hinge greatly on a well-designed population similarity and an efficient ant movement rule.

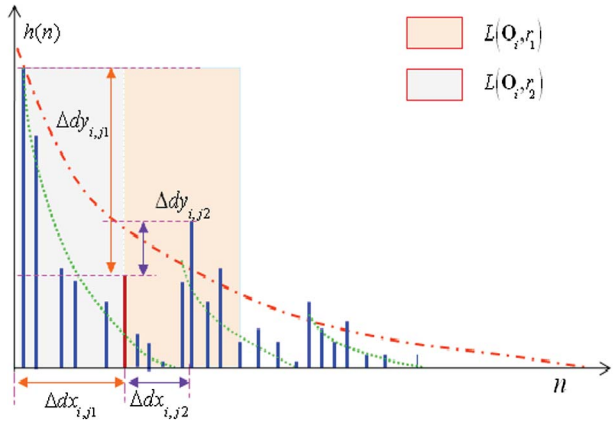


Fig. 1. The illustration of the formulated cluster identification problem on a two-dimensional amplitude and time of arrival plane.

### *B. Population Similarity*

To get these intelligent agents ahead on, firstly a proper environment similarity should be specified for the considered cluster identification problem [29]–[31]. Such an environmental fitness is supposed to effectively characterize the similarity of two considered MPCs, which may be thought of a rough probability of MPCs belonging to one single cluster. Usually, a reasonable environment similarity may produce fair data clustering results. In order to develop a good environment similarity, two practical considerations should be taken into accounts.

Firstly, it is apparent that, the closer the two MPCs' amplitudes coming to each other, the higher the probability of two MPCs coming from one unique cluster. We may denote the Euclidean distance between the two considered amplitudes by $\Delta dy_{i,j} = \left|y_i^{(k)} - y_j^{(k)}\right|$, for $\boldsymbol{O}_j^{(k)} \in L\left(\boldsymbol{O}_i^{(k)}, r\right)$. Accordingly, $\Lambda_r\left(\boldsymbol{O}_i^{(k)}, \boldsymbol{O}_j^{(k)}\right)$ is expected to decrease with the increasing of $\Delta dy_{i,j}$. To facilitate the algorithm design, in practice, a reciprocally decaying metric may be suggested to instinctively depict this relationship, i.e., $\Lambda_r\left(\boldsymbol{O}_i^{(k)}, \boldsymbol{O}_j^{(k)}\right) \propto \frac{1}{\Delta dy_{i,j}}$. Another more effective alternative, however, may be $\Lambda_r\left(\boldsymbol{O}_i^{(k)}, \boldsymbol{O}_j^{(k)}\right) \propto exp(-\Delta dy_{i,j})$. It is seen that, actually, the term $exp(-\Delta dy_{i,j})$ may give an exponentially distributed likelihood that the $i$th agent and the $j$th agent belong to one single group (or cluster).

Secondly, the closer the ToAs of two MPCs, the higher the probability of the two MPCs affiliated with the same cluster. Denote the Euclidean distance between two corresponding ToAs by $\Delta dx_{i,j} = \left|x_i^{(k)} - x_j^{(k)}\right|$ for $\boldsymbol{O}_j^{(k)} \in L\left(\boldsymbol{O}_i^{(k)}, r\right)$, thus $\Lambda_r\left(\boldsymbol{O}_i^{(k)}, \boldsymbol{O}_j^{(k)}\right)$ is also expected to be decreased as $\Delta dx_{i,j}$ increases. Similarly, we may assign $\Lambda_r\left(\boldsymbol{O}_i^{(k)}, \boldsymbol{O}_j^{(k)}\right) \propto exp(-\Delta dx_{i,j})$.

Combining the above two considerations together, we may define two environment similarities (corresponding respectively to the left and right region) as (5) and (6), shown at the bottom of the page. Here, $L\left(\boldsymbol{O}_i^{(k)}, r_1\right) = \left\{\boldsymbol{O}_j^{(k)} \middle| 0 < x_i^{(k)} - x_j^{(k)} \le r_1\right\}$ denotes the left neighborhood region of the $i$th agent $\boldsymbol{O}_i^{(k)} (i = 0, 1, 2, \ldots, N-1)$, where the $x$-values (on 2-D workspace) of all elemental agents are equal or smaller than $x_i^{(k)}$ by $r_1$, while $L\left(\boldsymbol{O}_i^{(k)}, r_2\right) = \left\{\boldsymbol{O}_j^{(k)} \middle| 0 < x_j^{(k)} - x_i^{(k)} \le r_2\right\}$ designates the right neighbors, which have also been illustrated by Fig. 1. In practice, we may simply have $r_1 = r_2 = r$. Notice that, $p(k)$ and $q(k)$ respectively account for the relative weights on two considered factors (i.e., ToA and amplitude of MPCs) during the $k$th iteration. And usually, we have $p(k) + q(k) = 1$ for all $k$. It is clearly seen that the weighting parameter $p(k)$ (or $q(k)$) gives a relative preference to two large-scale factors, which may have some impacts on the performance of cluster identifications. Their practical configurations will be lately discussed in Section III-D.

From (5) and (6), it is suggested that $\Lambda_{r_1}\left(\boldsymbol{O}_i^{(k)}\right)$ may roughly describe the probability that the current $i$th ant agent (or MPC) belongs to its left region $L\left(\boldsymbol{O}_i^{(k)}, r_1\right)$, while $\Lambda_{r_2}\left(\boldsymbol{O}_i^{(k)}\right)$ approximates the likelihood affiliated with the right one $L\left(\boldsymbol{O}_i^{(k)}, r_2\right)$. Given the defined environment similarity, the main objective of cluster identification is now to determine a sequence of most appropriate time-bounds which could divide the $x$-axis into multiple *non-overlapped* regions (i.e., clusters). Correspondingly, agent movements may be simplified to moving towards the most probable region (i.e., left or right).

$$\Lambda_{r_1}\left(\boldsymbol{O}_i^{(k)}\right) \triangleq \sum_{\boldsymbol{O}_j^{(k)} \in L\left(\boldsymbol{O}_i^{(k)}, r_1\right)} \frac{1}{p(k) \times exp(\Delta dx_{i,j}) + q(k) \times exp(\Delta dy_{i,j})} \tag{5}$$

$$\Lambda_{r_2}\left(\boldsymbol{O}_i^{(k)}\right) \triangleq \sum_{\boldsymbol{O}_j^{(k)} \in L\left(\boldsymbol{O}_i^{(k)}, r_2\right)} \frac{1}{p(k) \times exp(\Delta dx_{i,j}) + q(k) \times exp(\Delta dy_{i,j})} \tag{6}$$

Based on the above analysis, we may further define the movement preference as

$$\Lambda_r\left(\boldsymbol{O}_i^{(k)}\right) \triangleq \frac{\Lambda_{r_1}\left(\boldsymbol{O}_i^{(k)}\right)}{\Lambda_{r_2}\left(\boldsymbol{O}_i^{(k)}\right)}. \tag{7}$$

Accordingly, the current $i$th agent will migrate to the left region $L\left(\boldsymbol{O}_i^{(k)}, r_1\right)$ when the evaluated preference $\Lambda_r\left(\boldsymbol{O}_i^{(k)}\right)$ is larger than 1, while it will move into the right region if $\Lambda_r\left(\boldsymbol{O}_i^{(k)}\right) < 1$.

Although we have taken both the amplitude (i.e., $\Delta dy_{i,j}$) and ToAs (i.e., $\Delta dx_{i,j}$) into the population similarity, a simple moving strategy mentioned above, e.g., only towards the left or the right, seems still to be inefficient. First, the left (or right) region specified by the region resolution $r_1$ (or $r_2$) may cover a very broad range. For example, the single left region of the $i$th agent may even span from $x = 0$ to $x_i^{(k)}$. How to efficiently move round on this broad region and formulate some clusters as soon as possible, therefore, still remains as a key challenge. Second, the amplitude information should be jointly updated, which may further contribute to the population evolution during the next round. In order to maximize the functioning of the population-based clustering procedure, in fact, the positive feedback enhancement of ant intelligence also calls for an efficient updating of both two components.

### C. Position Updating

As far as the rule of ant movements is concerned, most existing ACC algorithms may be less effective to the cluster identification scenario. Taking the recently developed ant-movement (AM) algorithm for example [32], each agent could only select its subsequent positions $\left(x_i^{(k+1)}, y_i^{(k+1)}\right)$ *randomly* from eight nearest neighbors of the current position $\left(x_i^{(k)}, y_i^{(k)}\right)$. To be specific, the continuous 2-D workspace has been divided into $N_x \times N_y$ discrete grids, and each candidate position should meet $\sqrt{\left(x_i^{(k+1)} - x_i^{(k)}\right)^2 + \left(y_i^{(k+1)} - y_i^{(k)}\right)^2} \leq 1$ (unit grid distance). It is found that such a random position updating scheme, which utilizes only the *point-to-point* distance information while ignoring others neighborhood agents, may easily become blind and less attractive, by resulting in more computation burden and time consumption. Thus, we will adopt a promising move strategy, which avoids ants' aimless movements and, simultaneously, may enhance the clustering performance.

To be specific, when the similarity measurement $\Lambda_r\left(\boldsymbol{O}_i^{(k)}\right)$ is larger than 1, the $i$th agent (or MPC) will migrate to the *center of mass* of its left neighbors specified by $L\left(\boldsymbol{O}_i^{(k)}, r_1\right) = \left\{\boldsymbol{O}_j^{(k)} \middle| 0 < x_i^{(k)} - x_j^{(k)} \leq r_1\right\}$. Otherwise, it may move towards the center of mass of the right neighbors $L\left(\boldsymbol{O}_i^{(k)}, r_2\right)$ if $\Lambda_r\left(\boldsymbol{O}_i^{(k)}\right) < 1$. By fully utilizing the *single-to-multiple* information of many neighbor agents, both the amplitude and ToA can be jointly updated in an efficient way. If $\Lambda_r\left(\boldsymbol{O}_i^{(k)}\right) > 1$, then the position of the $i$th agent will be updated by (8), (9).

$$x_i^{(k+1)} = \frac{1}{N_1^{(k)}} \sum_{\boldsymbol{O}_j^{(k)} \in L\left(\boldsymbol{O}_i^{(k)}, r_1\right)} x_j^{(k)}, \tag{8}$$

$$y_i^{(k+1)} = \frac{1}{N_1^{(k)}} \sum_{\boldsymbol{O}_j^{(k)} \in L\left(\boldsymbol{O}_i^{(k)}, r_1\right)} y_j^{(k)}. \tag{9}$$

where $k$ accounts for the iteration index; $N_1^{(k)}$ denotes the sub-population size of neighbor agents over $L_1\left(\boldsymbol{O}_i^{(k)}, r_1\right)$. Otherwise, i.e., $\Lambda_r\left(\boldsymbol{O}_i^{(k)}\right) < 1$, its position will be updated by

$$x_i^{(k+1)} = \frac{1}{N_2^{(k)}} \sum_{\boldsymbol{O}_j^{(k)} \in L\left(\boldsymbol{O}_i^{(k)}, r_2\right)} x_j^{(k)}, \tag{10}$$

$$y_i^{(k+1)} = \frac{1}{N_2^{(k)}} \sum_{\boldsymbol{O}_j^{(k)} \in L\left(\boldsymbol{O}_i^{(k)}, r_2\right)} y_j^{(k)}. \tag{11}$$

With the designed similarity and movement rule, neighbor agents with sharing properties will gather together gradually, further making the local similarity be reinforced during the next round, which is the so-called *positive-feedback* enhancement of ant behaviors [26]. Compared with traditional random walks based position updating (e.g., AM algorithm), the ant movement driven by a center of mass may accelerate the convergence of population evolutions, if further combined with the new environment similarity. As demonstrated, by exploiting in parallel the single-to-multiple information of large populations, the probability of falling into local optimums may be also reduced [29].

Notice that, in the 1st round, the initial positions of ant-agents correspond exactly to their ToAs and amplitudes of input CIRs, i.e., $\left(x_i^{(0)}, y_i^{(0)}\right) = (t_i, \alpha_i)$. In the projection process, the maximum MPC amplitudes (i.e., $y_i^{(k)}$) have been normalized to 1, and the unity of such normalized amplitudes may be considered as the *Voltage*. Similarly, the time delays (i.e., $x_i^{(k)}$) have also been normalized by the sampling time, and the unity of such discrete indexes can be regarded as the *Second*. After MPCs being projected onto a 2-D workspace, then the unities of both two components are ignored (or treated as *One*), and the Euclid distance between any two virtual *objects* is concerned.

### D. Parameters Configuration

As suggested by most recent experiments carried in closed aircraft cabins [33], [34], the measure of UWB CIRs often requires a spatial averaging in order to eliminate the small-scale fading. It is achieved usually by repeating measurements within a uniform grid (i.e., spaced at least equal to half of the wavelength) [4], [35]. In practice, approximately 9 spatial grid samples will be sufficient to average out realistic small-scale fading effects [3].

On the other hand, a robust cluster identification scheme is also supposed to be relatively immune to the small-scale fading, especially when those spatial or physical mitigation mechanics

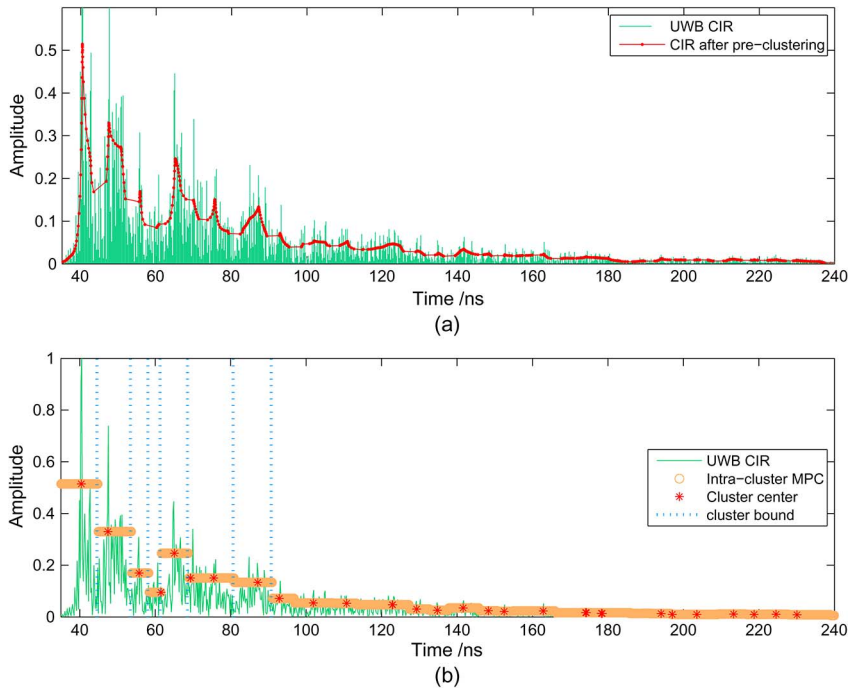


Fig. 2. (a) The derived result after the pre-clustering process with $k_0$ assumed to be 5. (b) Cluster identification result after 50 iterations. Note that, the intra-cluster MPCs are clustered onto several clusters with the clustering center denoted by red stars.

(e.g., grid measurements) are unavailable. For example, in certain circumstances the channel characteristic may become time-variant among grid measurements. In this case, a time-domain averaging (or moving averaging) process could be used to suppress unfavorable fading effects and thereby improve the cluster identification, as have been demonstrated by [18]–[20].

In this work, by properly configuring two relative weights $p(k)$ and $q(k)$, this problem will be addressed alternatively by the presented ant-based biological framework. In order to accomplish the objective of time-averaging, we may initially set $p(k) = 0$ and $q(k) = 1$ for a small $k \leq k_0$. Thus, with the agents moving towards the center of mass of neighbor populations, the local averaging on amplitudes may be implemented and, correspondingly, some specula reflections with strangely high amplitudes may be eliminated. During realistic analysis, the number of times of this pre-clustering (i.e., $k_0$) may be configured to 5$\sim$10. In fact, the pre-clustering procedure can be viewed as a special *filtering* mechanic. In sharp contrast to classical finite impulse response (FIR) filters with linear weights on MPCs, such a non-linear mechanic may remove the small-scale fading effectively, while preserving some subtle large-scale structures, as illustrated by the experimental result in Fig. 2(a). Due to the randomly distributed initial agents and complex population collaborations, it may be infeasible to exactly figure out how many paths have "moved" to nearby mass centers. It seems that, after the pre-clustering, many specula reflections will be smoothed by the agents' movement driven by the center-of-mass of neighborhood regions, as shown by Fig. 2(a).

Note that, despite the benefits of removing specula reflections, as a double-edge sword, such average operations may also smooth some real cluster points inevitably. In practice, a compromise should be made between false clusters (generated by small fading effects) and missing clusters (smoothed by averaging process). It is observed from the subsequent experiments that, with a relatively small pre-clustering resolution, fortunately the pre-clustering scheme will eliminate small-scale fading effects while generally preserving real cluster start-points.

Then, both the amplitude and ToAs should be considered during subsequent clustering process. In [36], ToAs are assumed to be a hidden Markov modeling (HMM), based on which cluster identifications of S-V channels are realized. By ignoring the amplitude discontinuity, unfortunately, the recovered clusters may overlap with each other. Thus, despite the significant theoretical contribution, this method can be hardly applied to channel modeling or the practical design, in which a channel response is also supposed to be impractically sparse [36]. In fact, as highlighted by [17] and [20], amplitude discontinuities usually involve useful information to judge a cluster [37]. In this scheme, we manage to make full use of the decaying property of amplitudes, yet still consider ToAs as the indispensable information for successful cluster identifications. Accordingly, we may practically set $p(k)$ to a constant $p$ for $k > k_0$.

Thus, the relative weight $p(k)$ can be configured as in eq. (12).

$$p(k) = \begin{cases} 0 & 1 < k \leq k_0, \\ p & k > k_0. \end{cases} \tag{12}$$

*1) Region Resolution Adaptation:* Since the similarity is evaluated within the neighbor region, the resolution parameters ($r_1$ and $r_2$) may also have impacts on clustering results. Practically, a larger resolution should be suggested at the beginning, in order to explore the whole space and avoid being attracted

by local optimum. As the clustering process continues, the resolution should be gradually shrunk to speed up the clustering convergence and form some clear inter-cluster bounds.

**Algorithm 1** Ant Intelligence-Based Cluster Identification

**Input**: Discrete UWB CIR $h(n)$
Guiding parameters $(p, r_p, r_0, \lambda)$
**Output**: A Data Clustering Result: $\mathcal{B} = \{b_i | i = 1, \cdots, I\}$

Project each MPC into the $x-y$ plane (i.e., 2-D virtual workspace). Initialize the pre-clustering times $k_0$, the initial region resolution $r_0$.
**for** $k \to 1$ to $k_0$ **do**
  Set the region resolution $r = r_0$, and the relative weight $p(k) = 0$, i.e., $q(k) = 1$.
  **for** $i \to r$ to $n - r$ **do**
    Calculate two environment similarities of the $i$th virtual ant, i.e., $\Lambda_{r_1}(\boldsymbol{O}_i^{(k)})$ and $\Lambda_{r_2}(\boldsymbol{O}_i^{(k)})$, and further obtain the movement preference $\Lambda_r\left(\boldsymbol{O}_i^{(k)}\right)$ according to eqs. (5)–(7).
    **if** $\Lambda_r\left(\boldsymbol{O}_i^{(k)}\right) \geq 1$ **then**
      Update the ant position $\boldsymbol{O}_i^{(k)}$, by moving it to the center of mass of its left neighbor according to eqs. (8) and (9).
    **else**
      Update the ant position $\boldsymbol{O}_i^{(k)}$, by moving it to the center of mass of its right neighbor according to eqs. (10) and (11).
    **end if**
  **end for**
**end for**
Reconfigure the relative weight $p(k)$ to $p$.
**for** $k \to k_0 + 1$ to $K$ **do**
  **for** $i \to r$ to $n - r$ **do**
    Calculate two environment similarities of the $i$th virtual ant, i.e., $\Lambda_{r_1}(\boldsymbol{O}_i^{(k)})$ and $\Lambda_{r_2}(\boldsymbol{O}_i^{(k)})$, and further obtain the movement preference $\Lambda_r\left(\boldsymbol{O}_i^{(k)}\right)$ according to eqs. (5)–(7).
    **if** $\Lambda_r\left(\boldsymbol{O}_i^{(k)}\right) \geq 1$ **then**
      Update the ant position $\boldsymbol{O}_i^{(k)}$, by moving it to the center of mass of its left neighbor according to eqs. (8) and (9).
    **else**
      Update the ant position $\boldsymbol{O}_i^{(k)}$, by moving it to the center of mass of its right neighbor according to eqs. (10) and (11).
    **end if**
  **end for**
  Update the region resolution $r = \lambda \times r$.
**end for**
Extract the clustering bound $b_i$ $(i = 1, \cdots, I)$, i.e., $b_i = \min\{x_k | \boldsymbol{O}_k \in i, k = 0, 1, \cdots, K_i - 1\}$.
Return the identified clusters breakpoints $\mathcal{B} = \{b_i\}$.

For simplicity, given the initialization resolution $r^{(0)} = r_1^{(0)} = r_2^{(0)}$, we may reduce it geometrically by using (13).

$$r^{(k)} = \begin{cases} r_p & 1 < k \leq k_0, \\ \lambda^{(k-k_0)} \times r^{(0)} & k > k_0. \end{cases} \tag{13}$$

Here, the pre-clustering resolution $r_p$ specifies the sensing range of ant agents in the pre-clustering stage. In order to derive accurate cluster identification results, in the 2nd stage, the attenuation constant $\lambda$ and the initial resolution $r^{(0)}$ should be configured properly. Later, the parameters will be configured based on experimental investigations. With such a resolution adaptation, the ant movement may usually produce promising identification results as shown by Fig. 2(b).

### E. Implementations

Based on the elaborations above, the proposed cluster extraction scheme has been summarized in the following **Algorithm** flowchart.

## IV. Numerical Simulations and Performance Evaluations

In this section, we will firstly evaluate the proposed cluster identification scheme with simulated UWB CIRs, which are generated from the channel model regulated by IEEE 802.15.4a TG [3], [4], [10]. Then, the new scheme will be further applied to measured UWB CIRs.

### A. Parameter Configurations

We firstly investigate the parameters configuration of this new ACC scheme. It is worth noting that, due to complicated collaborative mechanics of the large population, the theoretical analysis on parameters influence becomes practically intractable for most biological processes. Alternatively, we tend to derive the performance by resorting to the numerical approach. In the simulation, two performance metrics are mainly concerned, i.e., the mean error and the complexity. The first one is defined as the relative error (or derivation) between the identified starts and real clusters, which is also normalized by the average cluster interval. The second one accounts for the implementing computation of the designed ACC scheme, which may be roughly measured by the total number of accumulated iterations. With the numerically derived two metrics, the compromise should be made in practice and, accordingly, the feasible parameter settings can be determined.

In Fig. 3(a), the influences of the relative weight $p$ (and $q$) on both the mean error and the search complexity are demonstrated. Note that, the other weight $q = 1 - p$ will vary with $p$. UWB CIRs are generated from the CM5 model and, for the ACC process, the related parameters $(\lambda, r_p, r_0)$ are configured to (0.95, 1.5 ns, 7.5 ns). It is easily seen that the relative weight $p$ only has some effects on the identification performance, while is basically independent of the time complexity (or the accumulated search rounds). Based on the derived statistic results, it may be conclude that, for the CM5 channel, $p$ could be practically set to 0.6 which minimizes the mean derivation of identified clusters.

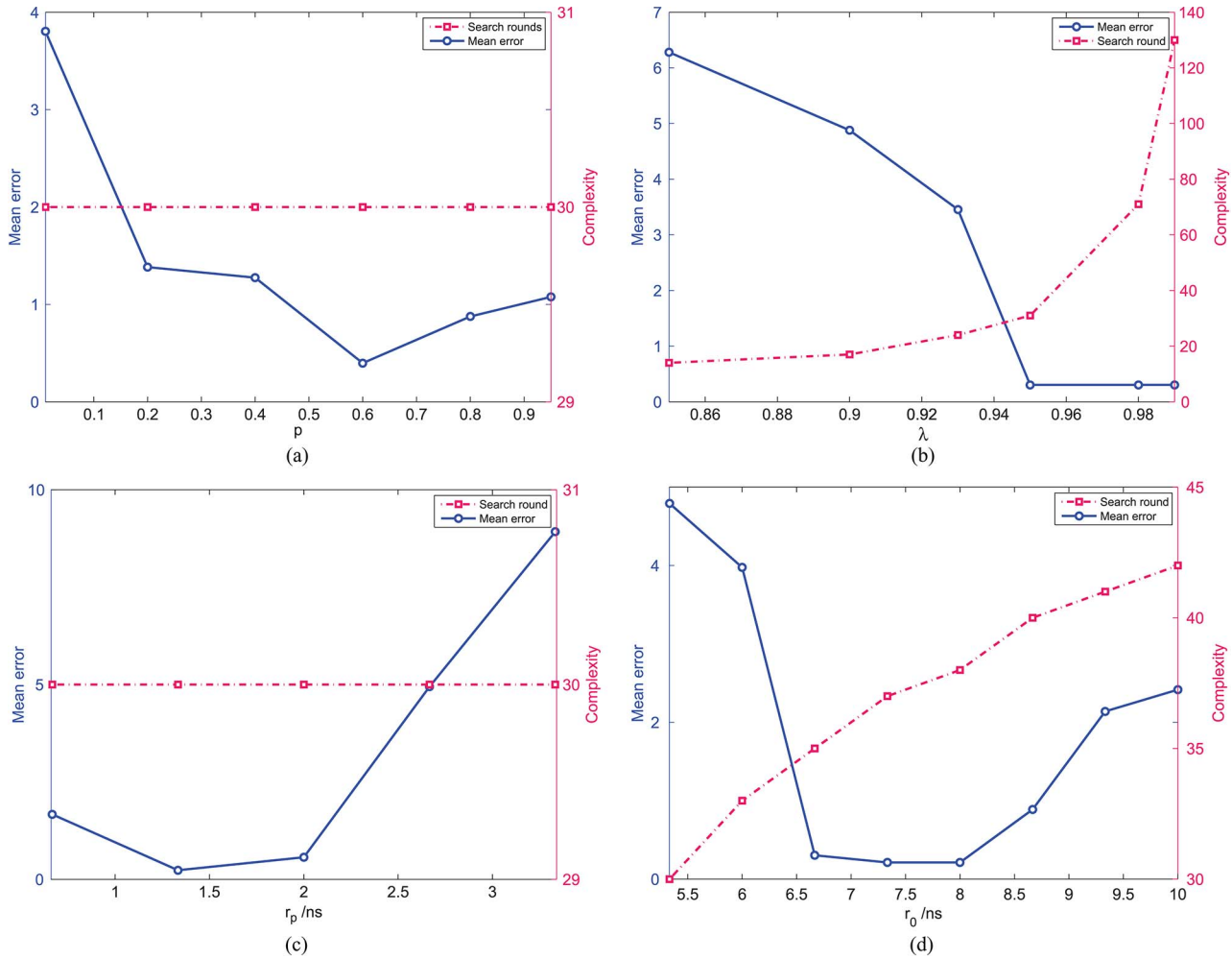


Fig. 3. Cluster identification performance under different parameters. (a) The relative weight $p$; (b) the decay constant $\lambda$; (c) the pre-clustering region resolution $r_p$; (d) the region resolution $r^{(0)}$. Note that, here the resolution parameters $r_p$ and $r_0$ account for the times.

We then evaluate how the decay constant $\lambda$ affects the cluster identification performance in the second experiment, in which the relevant parameters $(p, r_p, r_0)$ are configured to (0.7, 1.5 ns, 7.5 ns). From Fig. 3(b), the decay parameter $\lambda$ will have a noticeable effect on the search complexity. In practice, a larger $\lambda$ comes also with a slower region shrinking process, which may therefore slow down the convergence speed. If the fast region shrink is adopted (i.e., a small $\lambda$ is used), on the other hand, the search process will be accelerated excessively, which may lead to the deteriorated performances (e.g., the finding of local solutions). It is observed that if $\lambda$ is larger than 0.95, then the mean error seems to change little, whereas the search complexity will be increased dramatically. Thus, the decay parameter $\lambda$ may be properly chosen to 0.95.

In Fig. 3(c), the effects from the pre-clustering resolution $r_p$ are illustrated. In this simulation, the parameters $(p, \lambda, r_0)$ are configured to (0.7, 0.95, 7.5 ns). Apparently the algorithm complexity will not be influenced by the pre-clustering resolution $r_p$. Such a parameter, however, will affect the mean error of identified clusters. As has been mentioned, with a too small $r_p$, the fading effect may be suppressed insufficiently which will deteriorate the performance, while the cluster breakpoints will be smoothed and some separable clusters may be deviated by a too large $r_p$. From the experimental result, $r_p$ may be configured to 1.33–1.67 ns (approximately 4–6 samples) in order to primarily minimize the mean derivation.

Since the presented iterative scheme terminates when the neighbor region is small enough, e.g., $r^{(k)} < 3 \times t_s$ (sample time), a large initial region $r_0$ may increase the search complexity substantially, as demonstrated by Fig. 3(d). Here, $(p, \lambda, r_p)$ are configured to (0.7, 0.95, 1.5 ns). By extending the sensing range of agents, a large initial region may also fail to resolve some real clusters that are very close. A small $r_0$, on the other hand, may result in local solutions. Thus, the initial resolution $r_0$ should be configured carefully in order to obtain the promising identification performance while maintaining an acceptable complexity. Based on the numerical results, $r_0$ may be properly set to 6.67–8 ns (i.e., approximately 20–24 samples) in practice.

In the above experiments, the proposed cluster identification scheme is mainly exemplified by simulated CIRs of the CM5 channel, which usually exhibits distinct clusters and, therefore, allows to clearly visualize the algorithm performance. It is noteworthy that the parameters configuration, however, is practically associated with different types of simulated channels with various time resolutions and cluster properties (e.g., sparser

TABLE II
PARAMETERS CONFIGURATIONS OF CM1–CM8 SIMULATED CHANNELS

| CIRs Types | $p$ | $r_p$ | $r_0$ | $\lambda$ |
|---|---|---|---|---|
| CM1 | 0.4-0.6 | 0.25-0.38 ns | 1-1.25 ns | 0.94-0.96 |
| CM2 | 0.3-0.4 | 0.25-0.38 ns | 0.5-0.75 ns | 0.94-0.95 |
| CM3 | 0.2-0.3 | 0.67-1.00 ns | 4.67-6 ns | 0.95-0.96 |
| CM4 | 0.2-0.3 | 0.67-1.00 ns | 1-2 ns | 0.94-0.95 |
| CM5 | 0.5-0.7 | 1.33-1.67 ns | 5-8 ns | 0.95-0.96 |
| CM6 | 0.7-0.8 | 1.33-1.67 ns | 12.67-14 ns | 0.95-0.96 |
| CM7 | 0.5-0.7 | 0.17-0.33 ns | 2.67-3 ns | 0.95-0.96 |

or denser). As a consequence, the parameters configuration is also supposed to vary from different channel types. Based on experimental investigations and the similar criterion above, the feasible ranges of ACC's parameters under CM1–CM7 channels have been obtained, as summarized in Table II.

With regards to the above analysis, there are some other remarks worthy of note:

1) In the experimental simulation, only with a full exploration of the 4-dimension (4-D) parameters space can the optimal parameter configurations be derived. As far as a 4-D space is considered, unfortunately the involved implementing complexity of joint parameters evaluation may be unaffordable. For each possible parameter combination in the 4-D space of each single channel type, about 100 UWB CIRs may be required to derive numerical identification performances. The average number of clusters may approach 10 in each CIR, and during every experiment, some visual assistance may be needed. Even if each continuous parameter is represented by 20 discrete grids on its feasible range, such a complexity may easily become prohibitive.
2) To avoid the unaffordable complexity, rather than evaluating these four parameters jointly, a simplified approach is adopted. By searching along 4 separate directions, the experimental investigation may be feasible. It should be noteworthy that, even with a reduced optimization space, the considered parameters set has already been pre-screened or pre-evaluated. In other words, some bad parameters combinations or regions (e.g., $\lambda<0.8$ or $p\geq0.9$) have been preliminarily excluded. Consequently, the other fixed 3 parameters may be involved by a near-optimal (or at least local optimal) region. From numerical results, it is observed that promising identification performances have been obtained. Meanwhile, the performance variations under each parameter seem to remain within a relatively small region. Taking the initial resolution $r_p$ for example, given the pre-screened and fixed parameters set (i.e., $p = 0.7$, $r_0 = 5$ ns, $\lambda = 0.95$), a worst mean error is about 4.79%, while the near optimal (or sub-optimal) mean error is about 0.31%. Thus, the simplified optimization approach, i.e., a rough screening on parameters set followed by a local exhaustive search, may generally acquire the promising performances in practice (e.g., with the very small mean errors). It is expected that, with a more complicated 4-D full search, the identification performances may be further promoted. However, compared with the inaccessible low bound of 0, the identification errors achieved by the simplified scheme (e.g., 0.0031) may be sufficiently applicable to the realistic measurement analysis (e.g., parameters extraction) or channel modeling. Besides, the dependence between three guiding parameters, i.e., the initial resolution $r_0$, the relative weight $p$ and the pre-clustering resolution $r_p$, which are not explicitly connected with each other, can be identified by this simplified search process. From Fig. 3(a), (c), and (d), the curves of mean deviations of three parameters remain much similar to each other, i.e., first decreased and then increased. Supposed that the practical objective surface is continuous (or at least locally continuous), it may indicate that a correlation region (with similar trends on three parameters) exists in the high-dimensional surface.

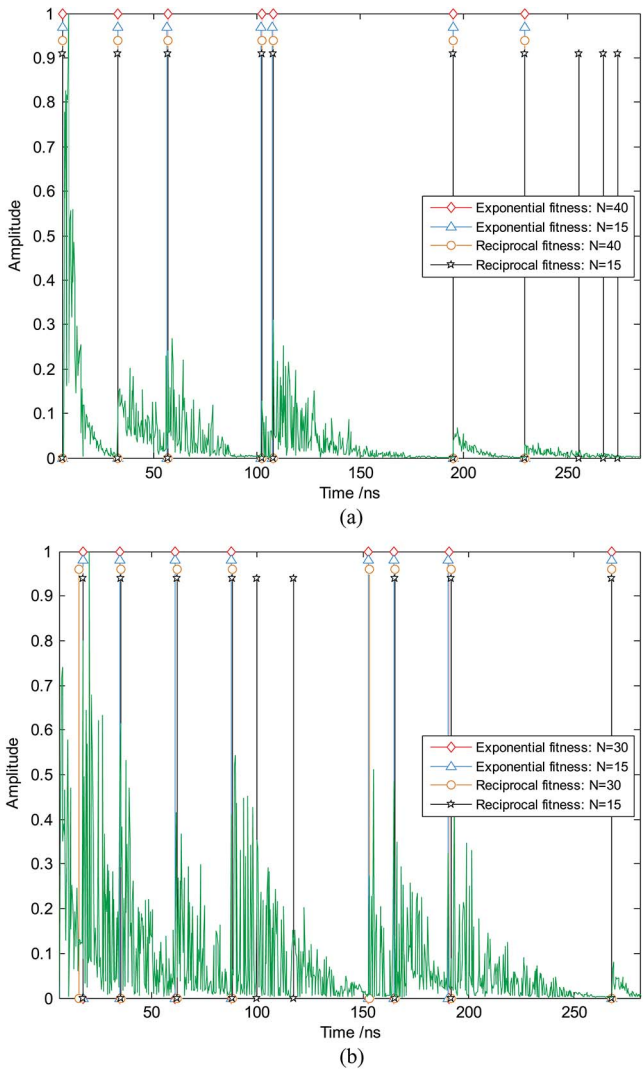


Fig. 4. Cluster identification results under different similarity. (a) LoS case; (b) NLoS case.

## B. Exponential or Reciprocal Metric?

The identification results under two feasible similarity metrics, i.e., the exponential metric and reciprocal metric, have been shown by Fig. 4. It is seen that, when the iterative

generation of ACC process is sufficiently large (e.g., $N = 40$), both the exponentially decaying metric and the reciprocally decaying metric can identify multiple clusters in an automatic manner. Actually, the identification results derived from two biological metrics are almost the same in this case. If the biological iteration is too small (for example $N = 15$), it is observed that the exponentially decaying metric may still produce clustering results as accurate as the large iteration case (e.g., $N = 40$). Due to inadequate clustering, however, the reciprocally decaying metric may produce unsatisfactory identification results. From the two specific realizations in Fig. 4, a shorter convergence time is required by the exponential metric. It is shown from extensive experiments that the exponential metric is of some efficiency in CM5 channels. Similar observations can be made to CM6 and CM7 channels.

Naturally, the Gaussian metric can be also suggested in practice, i.e., $\Lambda_r\left(\boldsymbol{O}_i^{(k)}, \boldsymbol{O}_j^{(k)}\right) \propto exp(-\Delta x_{i,j}^2)$. We found that, nevertheless, a faster decaying metric is not always necessary to have a better performance. In order to obtain a more competitive performance, the optimal metric should also conform to realistic distributions of MPCs in the 2-D workspace. Thus, the similarity metric will even become correlated with specific CIR realizations of different cluster property. How to determine exact effects of different metrics on different channel types, therefore, remains still as an interesting topic in future. For convenience, the exponential metric is suggested in the following analysis, which may basically produce promising clustering results.

### C. Cluster Identification Performance

Based on the above analysis, experimental results of various simulated CIRs have been shown in Fig. 5. It is seen that, for CM1∼CM7 channels, the presented scheme can identify multiple clusters in UWB CIRs automatically. From Fig. 5(h), however no clear bound can be finally formed after the clustering procedure, i.e., the ACC based scheme fails to identify clusters in CM8 channels. In fact, the resolvable MPCs of this extreme NLOS scenario, which are measured with an infinite time resolution (or huge bandwidth) and in dense multipath environments, may be very close and the MPCs' amplitude becomes comparable in neighbor regions. The ant-agent will move around but fail to gather together and, as a consequence, no explicit MPCs group will be resolved even by the biological procedure. In this complex situation, it is more likely (or reasonable) they will belong to one single cluster and the soft-onset shape in (4) is shown suitable to depict such single-cluster PDPs [4], [5]. In such soft-onset cases, it is impossible to identify clusters simply with time and amplitude information. An extension of the proposed approach, e.g., by including the direction of arrival (DoA) and direction of departure (DoD), may be able to distinguish multiple clusters.

The other two existing methods are also investigated in the context of CM5, i.e., the wavelet-based method in [20] and the piece-wise linear regression algorithm in [18]. It is apparent that, from Fig. 6, the proposed ACC scheme would accurately recognize cluster start-points. Due to the sensitive parameters configuration, nevertheless, the wavelet-based discontinuities detection scheme may sometimes exclude certain noticeable clusters. For example, the 4*th* cluster in Fig. 6(b) (located at 83 ns) has been missed. Meanwhile, by ignoring the important property of ToAs, such a scheme may produce several false clusters by mistaking some specula reflections for cluster break-points, e.g., the cluster located at 144 ns in the plotting of Fig. 6(a). Besides, the wavelet-based technique may shift the cluster start-points to certain maximum MPCs, due to the inaccurate averaging-based extraction [20]. The resulting deviated estimations may become noticeable especially when the first intra-cluster MPC is not the maximum one. For example, in Fig. 6(a), the estimated start-point of the 3*rd* cluster has been deviated dramatically. Another popular method, i.e., the linear regression technique, may suffer from sensitivity to the key parameters (e.g., the MPC interval and the MSE threshold) [18] and may fail to produce attractive identification performances [37]. Since simulated CIRs may not always strictly follow a negative exponential decay law, the extracted cluster-starts seem to also have deviations, as shown by Fig. 6. Note that, in numerical experiments, the involved parameters of two counterpart methods have been adjusted according to different channel types [18], [20].

Visual aspects may definitely provide a comprehensible view of identification performances. Such methods, however, lack of a quantitative description and, therefore, is not sufficient for convincing comparisons. In contrast, the statistical approach may be of significance to deeper understanding and more thorough performance evaluations. Based on the experiments, the cumulative distribution functions (CDFs) of the mean errors have been plotted. As shown by Fig. 7, from a point view of numerical fitting, a generalized extreme value (GEV) distribution may quite fit the CDF of the piecewise linear-regression method, while an exponential distribution seems to be more suitable to the wavelet method. For the presented ACC scheme, it is shown that a negative Binormal distribution can closely match its error CDF. From the statistical CDFs, it is seen the proposed method is superior to another two existing methods, as far as the mean deviation is concerned.

From the experimental result shown in Fig. 6, it is recognized that, unfortunately, the mean error of deviated estimations is no longer an effective criteria of performance evaluations in this cluster identification problem, especially when the missing cluster and the wrong cluster are considered. To remedy this problem, more profound quantitative measures should be exploited. As observed from experimental simulations, there may contain three kinds of errors in identified clusters, i.e., the missing clusters, the wrong clusters (or erroneously identified clusters) and the error clusters with start-point deviations. To make the analysis more precise, a tolerable error ratio, denoted by $\rho$, is employed to separate the error (or deviated) clusters and wrong clusters from the identification results. To be specific, (1) if the deviation of an estimated cluster start (i.e., $\hat{T}_l$) is smaller than $\rho$, i.e., $|T_l - \hat{T}_l| < \rho \times \frac{1}{\Upsilon}$, then it will be treated as an error estimation of the $l$th real cluster; (2) else if the derived cluster start $\hat{T}_l$ satisfies both $\hat{T}_l - T_l \geq \rho \times \frac{1}{\Upsilon}$ and $T_{l+1} - \hat{T}_l \geq \rho \times \frac{1}{\Upsilon}$, then it will be treated as a wrong cluster; (3) else if there is no estimation falls into the reference region $|T_l - \hat{T}_l| < \rho \times \frac{1}{\Upsilon}$, then the missing estimation occurs; (4) if several estimated cluster

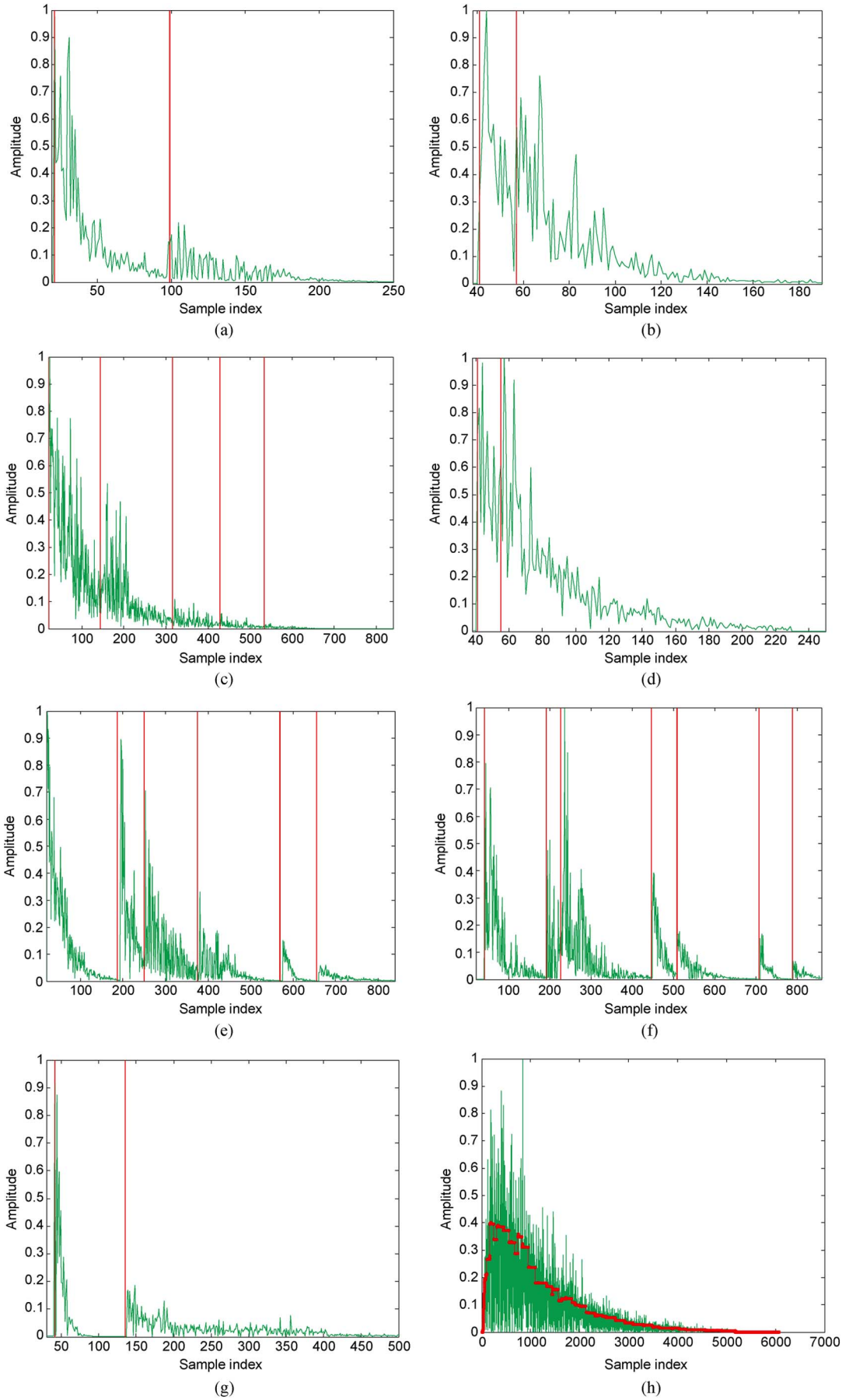


Fig. 5. Cluster identification results for the simulated UWB CIRs, i.e., CM1–CM8.

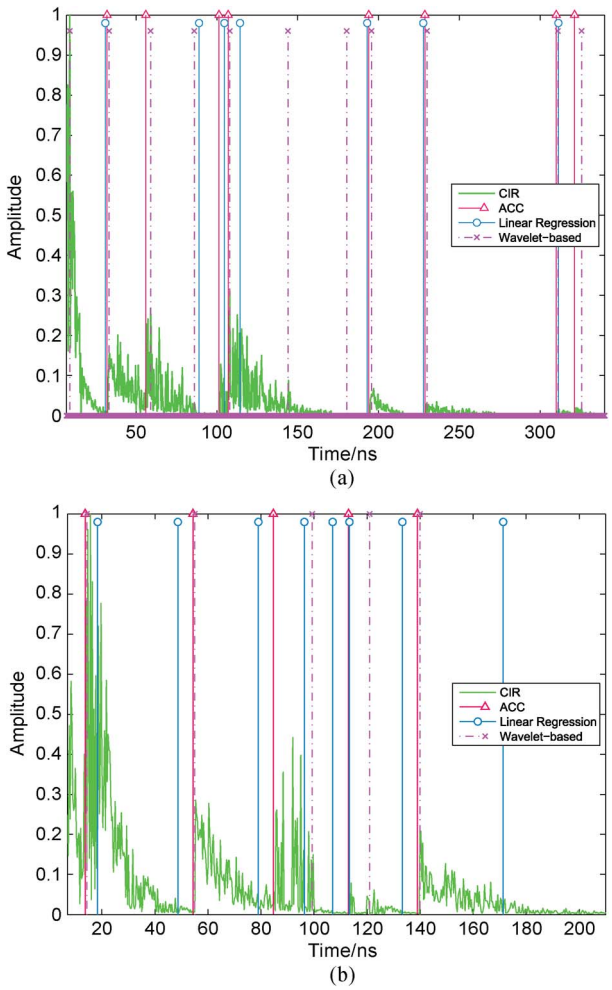


Fig. 6. Cluster identification results under different methods. (a) LoS case; (b) NLoS case.

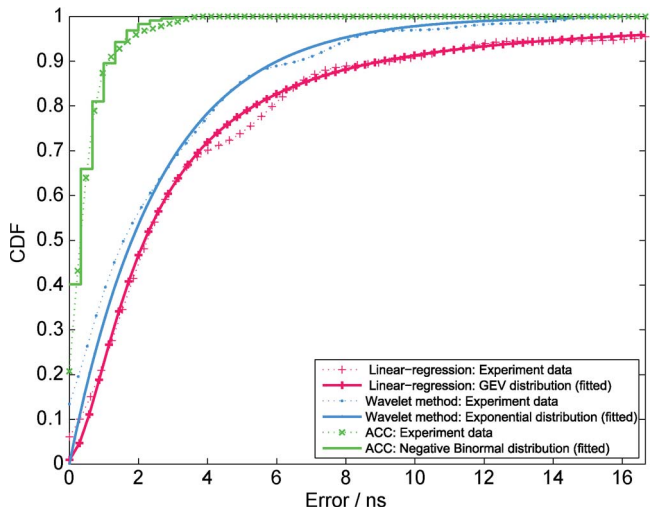


Fig. 7. The cumulative distribution functions of the deviation errors. Note that, the CIRs are simulated from the CM5 channel type in the experiment.

starts simultaneously meet $|T_l - \hat{T}_l| < \rho \times \frac{1}{\Upsilon}$, then the *closet* estimation with respect to the $l$th real cluster is considered as one error cluster, while the remaining estimations will be viewed as wrong clusters. In the experiment, the tolerable error ratio is configured to $\rho = 0.3$.

For the purpose of comparative analysis, four key statistic metrics, i.e., the probability of missing clusters $P_m$, the probability of wrong clusters $P_w$, the probability of error clusters $P_e$ and the relative error of mean deviations $\Delta E$, are estimated numerically, which are summarized in Table III. In order to estimate the above probabilities, three counters are employed to respectively record the numbers of three types estimations. Based on experimental simulations, then each probability is calculated from the occurrence ratio of the corresponding estimations. The mean error (or deviation) here, is obtained only from the error deviated clusters, i.e., by discarding the wrong cluster estimations. That is, $\Delta E \triangleq \mathsf{E}\{(T_l - \hat{T}_l) \times \Upsilon\} \times 100\%$ where each $\hat{T}_l$ meets $|T_l - \hat{T}_l| < \rho \times \frac{1}{\Upsilon}$.

From the derived results, it should be noteworthy that, for specific simulated channels, some performance measures of two classical methods may be comparable or even preferable to the new ACC scheme. For example, for the CM7 channels, the relative mean deviations of the linear-regression method and the ACC scheme are equal basically. Then, for the CM1 channel, the probabilities of error clusters (i.e., $P_e$) of both the linear-regression technique and the wavelet-based method are superior to ACC. And for the CM2 channel, the wrong clusters probability $P_w$ of the wavelet-based method is much lower than ACC. In addition, it is seen that one measure of the proposed ACC scheme, i.e., the probability of missing clusters $P_m$, may always surpass the other two methods in simulated channels. Based on the derived performance metrics, it may be therefore concluded that, in general, the ACC scheme would produce attractive identification results.

Note that, operating blindly on provided UWB CIRs, the identification performances of existing schemes (including the new ACC algorithm) are all dependent of different types of UWB CIRs (even different CIRs of the same type). In practice, CIRs of a good clustering quality will result in the promising identification result. CIRs of bad qualities, like simulated CIRs of CM1–CM4 channels (i.e., with indistinct clusters or polluted by small-scale fading effects), may lead to inaccurate estimations (e.g., producing more wrong and error clusters). For such CIRs, actually the cluster phenomenon is insignificant or some adjacent clusters may become seriously overlapped.

### D. Generalizations of Unknown Channels

Even the involved parameters have been investigated in different channels, the generalization of the new scheme to unknown channels (i.e., typically without *a priori* information) should also be considered, in order to make the designed algorithm more useful. First, as demonstrated by the above analysis, the parameters configuration should be compatible with specific CIRs in order to obtain the promising identification results if the prior knowledge is available, i.e., different channel types may have different parameters configuration. Second, we have to recognize a key point in designing more realistic algorithm that, rather than to seek the best parameter configurations for all situations, we have to find a general configuration approach alternatively when the *a priori* knowledge is unavailable, which

TABLE III
ESTIMATIONS PERFORMANCE OF DIFFERENT CLUSTER IDENTIFICATION METHODS

| Types of CIRs | Proposed Method | | | | Linear Regression | | | | Wavelet-based Method | | | |
|---|---|---|---|---|---|---|---|---|---|---|---|---|
| | $P_m$ | $P_w$ | $P_e$ | $\Delta E$ | $P_m$ | $P_w$ | $P_e$ | $\Delta E$ | $P_m$ | $P_w$ | $P_e$ | $\Delta E$ |
| CM1 | 5.25% | 1.15% | 42.11% | 4.29% | 55.56% | 1.25% | 20.83% | 6.83% | 52.89% | 2.63% | 21.05% | 4.8% |
| CM2 | 1.84% | 18.16% | 27.27% | 3.01% | 62.05% | 63.64% | 30.05% | 3.52% | 37.89% | 6.68% | 54.55% | 5.21% |
| CM3 | 1.72% | 2.76% | 17.24% | 2.02% | 24.13% | 10.32% | 37.92% | 6.63% | 24.14% | 3.45% | 31.03% | 10.09% |
| CM4 | 1.65% | 6.65% | 10.25% | 1.95% | 40.15% | 28.97% | 29.82% | 6.3% | 28.96% | 35.67% | 34.23% | 10.65% |
| CM5 | 0.57% | 0.61% | 2.49% | 1.59% | 15.56% | 10.28% | 35.77% | 11.83% | 5.96% | 12.68% | 24.14% | 7.11% |
| CM6 | 0.69% | 0.56% | 2.78% | 1.35% | 15.28% | 11.13% | 36.56% | 12.13% | 5.56% | 13.89% | 25.06% | 6.81% |
| CM7 | 2.78% | 8.33% | 8.33% | 4.45% | 13.89% | 11.08% | 11.12% | 4.74% | 24.53% | 2.78% | 22.24% | 7.25% |

may be then applied to most applications and produce sufficiently good (maybe not optimal) performances.

1) It seems that the decay constant $\lambda$ is basically independent of various different channels. The fact is that, in practice, a larger $\lambda$ may correspond to a slower population evolution, which, however, would exploits the underlying similarity property more profoundly and therefore produce more promising performances. Further taking the computational complexity, the parameter $\lambda$ may be set to 0.85∼0.95 for most UWB CIRs without any *a priori* information.
2) With the main objective of suppressing small-scale fading effects, another two parameters, i.e., the pre-clustering resolution $r_p$ and the relative weight $p$, seem to be associated with the fading property correspondingly. For a typical UWB bandwidth of 3∼5 GHz, it is recognized that the small-scale fading property is mainly related with operating environments. If no such prior information (e.g., scenarios) is available, $r_p$ may be set to 5–7 *discrete samples*, while $p$ can be configured to 0.5∼0.7.
3) By specifying the local resolution of each evolution, $r_0$ is associated with the interval of two adjacent clusters. In the analysis of realistic CIRs without any *a priori* information, $r_0$ can be determined according to the estimated minimum cluster interval $\Delta\hat{T}_m$. To be specific, in order to avoid smoothing the amplitude discontinuity of adjacent clusters, $r_0$ is supposed to remain smaller than $\Delta\hat{T}_m$. In practice, the minimum cluster interval $\Delta\hat{T}_m$ could be estimated based on several realistic channels with the assistance of observers.

Further, the designed ACC scheme is validated with realistic UWB measurements. The CIRs are obtained from the recent UWB measurement campaign [20], [22]. In the experiment, an indoor office room of $4.4 \times 2.5 \times 3.15$ m$^3$ is considered, typically involving a bookshelf, a desk and a flat panel display (FPD). The walls are made of the popular *acrylic-glass* material. Based on the *Agilent N5269 VNA*, a typical setup of the frequency-domain measurement is constructed. Two omnidirectional antennas working in 2.3∼11 GHz are adopted [20], with the voltage standing wave ratio (VSWR) less than 2.25 across the measurement band. The azimuth gain variation (AGV) is about ±1.25 dB. The vector network analyzer (VNA) sweeps unknown channel frequency response from 2.3 GHz to 11 GHz in 5600 linearly distributed points, i.e., the sweeping interval is about 1.55 MHz. Then, discrete UWB CIRs of 6∼9 GHz are extracted after some pre-processing operations (e.g., windowing, IFFT and deconvolution).

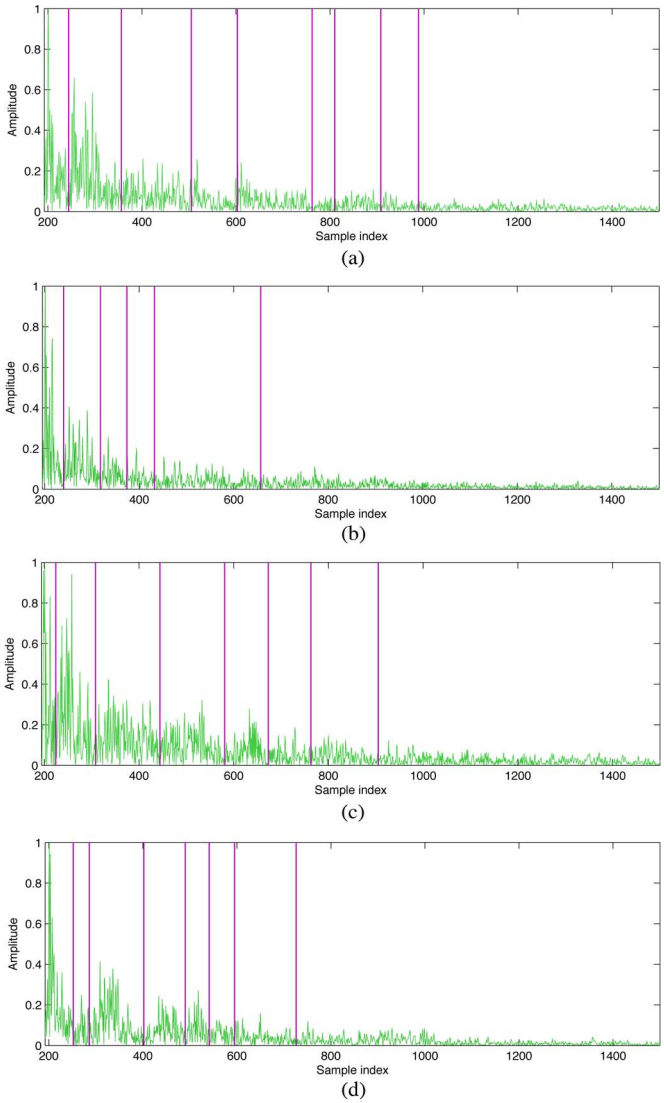


Fig. 8. Identification performance of realistic measurements.

The parameters of the ACC scheme are configured according to the above generalization analysis. In the experiments, $\lambda = 0.87$, $p = 0.7$, and $r_p = 6$ samples. The estimated minimum cluster interval $\Delta\hat{T}_m$ is about 40 samples, thus $r_0$ may be set to 38∼40 samples. From the derived results shown in Fig. 8, it is seen that multiple clusters in measured UWB CIRs can be automatically identified by the ACC scheme, which is hence applicable to unknown CIRs.

## V. Conclusion

A promising cluster identification algorithm for UWB propagations is developed. A new cluster identification formulation, relying on a novel conception of biological data clustering, is established. The resolvable MPCs are viewed as a group of ant-agents on a 2-D (i.e., amplitude and ToAs) virtual workspace, in which they are fully movable by sensing the local environment similarity. By constructing a novel population similarity that thoroughly exploits the decaying amplitude and ToAs characteristics, the cluster extraction, treated as a special data-clustering problem, is addressed elegantly by the biological ACC mechanic. Based on experimental simulations, the parameters configuration is investigated and a group of performance measures are numerically derived. As demonstrated, attractive identification performances can be obtained in most scenarios by the designed ACC scheme. Despite the accurate identification of cluster start-points, further distinguishing the overlapped intra-cluster MPCs still remains as an open area. Generally, the new scheme provides a compelling processing paradigm for cluster identifications in channel modeling, which allows the more profound understanding on realistic UWB propagations. Besides, the presented method may be also of great promise to other time-series analysis.

## Acknowledgment

We greatly thank anonymous reviewers for their constructive comments that allowed us to improve the paper significantly.

## References

[1] C. F. Mecklenbrauker *et al.*, "Vehicular channel characterization and its implications for wireless system design and performance," *Proc. IEEE*, vol. 99, no. 7, pp. 1189–1212, Jul. 2011.

[2] L. Q. Yang and G. B. Giannakis, "Ultra-wideband communications: An idea whose time has come," *IEEE Signal Process. Mag.*, vol. 21, no. 6, pp. 26–54, Nov. 2004.

[3] A. F. Molisch, "Ultrawideband propagation channels—Theory, measurement, and modeling," *IEEE Trans. Veh. Technol.*, vol. 54, no. 5, pp. 1528–1545, Sep. 2005.

[4] A. F. Molisch, "Ultra-wideband propagation channels," *Proc. IEEE*, vol. 97, no. 2, pp. 353–371, Feb. 2009.

[5] A. F. Molisch *et al.*, "A comprehensive model for ultra-wideband propagation channels," *IEEE Trans. Antennas Propag.*, vol. 54, no. 11, pp. 3151–3166, Nov. 2006.

[6] M. Z. Win and R. A. Scholtz, "Ultra-wide bandwidth time hopping spread spectrum impulse radio for wireless multiple-access communications," *IEEE Trans. Commun.*, vol. 48, no. 4, pp. 679–689, Apr. 2000.

[7] D. Cassioli, M. Z. Win, and A. F. Molisch, "The ultra-wide bandwidth indoor model: From statistical model to simulations," *IEEE J. Sel. Areas Commun.*, vol. 20, no. 6, pp. 1247–1257, Aug. 2002.

[8] A. Saleh and R. Valenzuela, "A statistical model for indoor multipath propagation," *IEEE J. Sel. Areas Commun.*, vol. 5, no. 2, pp. 128–137, Feb. 1987.

[9] J. R. Foerster, "IEEE 802.15.SG3a, Channel modeling sub-committee report final," Inst. Elect. Electron. Eng. Inc., New York, NY, USA, IEEE p802.15-02/490r1-SG3a, Feb. 2003.

[10] A. F. Molisch *et al.*, "IEEE 802.15.4a channel model—Final report," Inst. Elect. Electron. Eng. Inc., New York, NY, USA, IEEE 802.15-04-0662-00-004a, Nov. 2004.

[11] S. Adam, "Characterization of radio-wave propagation in indoor industrial environments," M.S. thesis, Simon Fraser Univ., Burnaby, BC, USA, 2010.

[12] W. Ciccognani, A. Durantini, and D. Cassioli, "Time domain propagation measurements of the UWB indoor channel using PN sequence in the FCC-compliant band 3.6–6 GHz," *IEEE Trans. Antennas Propag.*, vol. 53, no. 4, pp. 1542–1549, Apr. 2005.

[13] K. Haneda, J. Takada, and T. Kobayashi, "Cluster properties investigated from a series of ultra-wideband double directional propagation measurements in home environments," *IEEE Trans. Antennas Propag.*, vol. 54, no. 12, pp. 3778–3788, Dec. 2006.

[14] C. C. Chong, "S-V Parameter Extraction: General Guidelines," *IEEE 15-04-0283-00-004a*.

[15] C. Carbonelli and U. Mitra, "Clustered ML channel estimation for ultra-wideband signals," *IEEE Trans. Wireless Commun.*, vol. 6, no. 7, pp. 2412–2416, Jul. 2007.

[16] K. Witrisal *et al.*, "Noncoherent ultra-wideband systems," *IEEE Signal Process Mag.*, vol. 26, no. 4, pp. 48–66, Jul. 2009.

[17] O. H. Woon and S. Krishnan, "Identification of clusters in UWB channel modeling," in *Proc. IEEE VTC-Fall*, 2006, pp. 1–5.

[18] J. Chuang, S. Bashir, and D. G. Michelson, "Automated identification of clusters in UWB channel impulse responses," in *Proc. CCECE*, 2007, pp. 761–764.

[19] A. Massouri, L. Clavier, P. Combeau, and Y. Pousset, "Automated identification of clusters and UWB channel parameters dependency on Tx-Rx distance," in *Proc. 3rd EuCAP*, 2009, pp. 376–379.

[20] B. Li, Z. Zheng, D. J. Li, and S. J. Zhai, "Efficient cluster identification for measured ultra-wideband channel impulse response in vehicle cabin," *Progr. Electromagn. Res.*, vol. 117, pp. 121–147, 2011.

[21] H. Nikookar and R. Prasad, *Introduction to Ultra Wideband for Wireless Communications, Signals, and Communication Technology*. Berlin, Germany: Springer Science & Business Media B.V., 2009, pp. 164–171.

[22] B. Li, C. L. Zhao, H. J. Zhang, Z. Zheng, and X. B. Sun, "Characterization on clustered propagations of UWB in vehicle passenger cabin: Measurement, cluster identification and modeling evaluation," *IEEE Sensors J.*, vol. 14, no. 13, pp. 1288–1300, Nov. 2012.

[23] S. Roy, J. R. Foerster, V. S. Somayazulu, and D. G. Leeper, "Ultra wideband radio design: The promise of high-speed, short-range wireless connectivity," *Proc. IEEE*, vol. 92, no. 2, pp. 295–311, Feb. 2004.

[24] R. Bose, A. Freedman, and B. D. Steinberg, "Sequence CLEAN: A modified deconvolution technique for microwave images of contiguous targets," in *IEEE Trans. Aerosp. Electron. Syst.*, Jan. 2002, vol. 38, no. 1, pp. 89–97.

[25] P. G. Espejo and F. Herrera, "A survey on the application of genetic programming to classification," *IEEE Trans. Syst., Man, Cybern. C, Appl. Rev.*, vol. 40, no. 2, pp. 121–144, Mar. 2010.

[26] M. Dorigo, V. Maniezzo, and A. Colorni, "Positive feedback as a search strategy," Dip. Elettronica, Politecnico di Milano, Milano, Italy, Tech. Rep. 91-016, 1991.

[27] M. Dorigo, V. Maniezzo, and A. Colorni, "The ant system: Optimization by a colony of cooperating agents," *IEEE Trans. Syst., Man, Cybern. B, Cybern.*, vol. 26, no. 1, pp. 29–42, Feb. 1996.

[28] E. D. Lumer and B. Faieta, "Diversity and adaptation in populations of clustering ants," in *Proc. 3rd Int. Conf. Simul. Adaptive Behaviour: Animals Animats*, D. Cli, P. Husbands, J. Meyer, and S. Wilson, Eds. Cambridge, MA, USA: MIT Press, 1994, pp. 501–508.

[29] B. Li, Z. Zheng, and W. Z. Zou, "Ant intelligence inspired blind data detection for ultra-wideband radar sensors," *Inf. Sci.*, vol. 255, pp. 204–220, Jan. 2014.

[30] L. Zhang and Q. X. Cao, "A novel ant-based clustering algorithm using the kernel method," *Inf. Sci.*, vol. 18, no. 20, pp. 4658–4672, Oct. 2011.

[31] J. Handl, J. Knowles, and M. Dorigo, "On the performance of ant-based clustering," *Frontiers Artif. Intell. Appl.*, vol. 104, pp. 204–213, 2003.

[32] X. H. Xu, L. Chen, and Y. X. Chen, "A4C: An adaptive artificial ants clustering algorithm," in *Proc. IEEE Symp. Comput. Intell. Bioinformat. Comput. Biology*, 2004, pp. 268–274.

[33] L. C. Kin, J. Martin, and K. Thomas, "A systematic approach for UWB channel modeling in aircraft cabin," in *Proc. IEEE VTC-Fall*, Anchorage, AK, USA, 2009, pp. 1–5.

[34] S. Chiu, J. Chuang, and D. G. Michelson, "Characterization of UWB channel impulse responses within passenger cabin of a Boeing 737-200 aircraft," *IEEE Trans. Antennas Propag.*, vol. 58, no. 3, pp. 935–945, Mar. 2005.

[35] C. W. Kim, "Characterization of ultra-wideband channels for outdoor office environment," in *Proc. IEEE WCNC*, 2005, pp. 950–955.

[36] D. Shutin and G. Kubin, "Cluster analysis of wireless channel impulse responses with hidden Markov models," in *Proc. IEEE ICASSP*, May 2004, pp. 949–952.

[37] C. Gentile, "Automatic clustering of multipath arrivals in radio-frequency channels using kurtosis," in *Proc. IEEE ICC*, Budapest, Hungary, Jun. 2013, pp. 5726–5731.

**Bin Li** received the Bachelor's degree in electrical information engineering from Beijing University of Chemical Technology, Beijing, China, in 2007 and the Ph.D. degree in communication and information engineering from Beijing University of Posts and Telecommunications (BUPT), Beijing, in 2013. Since 2013, he has been a Lecturer with the School of Information and Communication Engineering, BUPT. He has published more than 60 journal and conference papers. His current research interests are focused on statistical signal processing algorithms for wireless communications, e.g., ultra-wideband, wireless sensor networks, millimeter-wave communications, and cognitive radios. Dr. Li served as a Regular Reviewer for the IEEE TRANSACTIONS ON COMMUNICATIONS, the IEEE TRANSACTIONS ON SIGNAL PROCESSING, and the IEEE TRANSACTIONS ON WIRELESS COMMUNICATIONS. He received the 2011 ChinaCom Best Paper Award and the 2010 and 2011 Excellent Ph.D. Student Award from BUPT Foundation.

**Chenglin Zhao** received the Bachelor's degree in radio technology from Tianjin University, Tianjin, China, in 1986 and the master's degree in circuits and systems and the Ph.D. degree in communication and information system from Beijing University of Posts and Telecommunications (BUPT), Beijing, China, in 1993 and 1997, respectively. He is currently a Professor with BUPT. His research is focused on emerging technologies of short-range wireless communication, cognitive radios, and 60-GHz millimeter-wave communications.

**Haijun Zhang** received the Ph.D. degree from Beijing University of Posts and Telecommunications (BUPT), Beijing, China. Currently, he is a Postdoctoral Research Fellow with the Department of Electrical and Computer Engineering, The University of British Columbia, Vancouver, BC, Canada, and he is also an Assistant Professor with the College of Information Science and Technology, Beijing University of Chemical Technology, Beijing. From September 2011 to September 2012, he visited the Centre for Telecommunications Research, King's College London, London, U.K., as a joint Ph.D. student and Visiting Research Associate. He has published more than 40 papers and authored 2 books. His current research interests include wireless resource allocation, 5G, heterogeneous small-cell networks, and ultradense networks. Dr. Zhang served as the Chair of the Technical Program Committee of the Game Theory in Wireless Communications Symposium of the 2014 International Conference on Game Theory for Networks (GAMENETS'14).

**Zheng Zhou** (M'05) received the Bachelor's degree in electrical engineering from Harbin Institute of Military Engineering, Harbin, China, in 1967 and the master's and Ph.D. degrees in electrical engineering from Beijing University of Posts and Telecommunications (BUPT), Beijing, China, in 1982 and 1988, respectively. Currently, he is a Professor with BUPT. From 1993 to 1995, he was a Visiting Research Fellow with the Department of Information Engineering, The Chinese University of Hong Kong, Hong Kong, supported by the Hong Kong Telecom International Postdoctoral Fellowship. From 1998 to 2003, he was also the Vice Dean of the School of Telecommunication Engineering, BUPT, and in 2000, he was the Invited Overseas Researcher at Japan Kyocera DDI Future Communication Research Institute (supported by Japan Key Technology Center). Prof. Zhou served as a member of the Technical Committee on Cognitive Networks of the IEEE Communications Society, the International Steering Committee Member of the IEEE International Symposium on Communications and Information Technologies (ISCIT) in 2003–2010, and the TPC Cochair of the IEEE ISCIT 2005. He was also the General Vice Chair of the IEEE ChinaCom 2006 (the first international conference on communications and networking in China) and a Steering Committee Member of IEEE ChinaCom 2007. He is a Voting Member and Contributor of the IEEE 802.15 Task Group (TG3a and TG4a), a Senior Member of China Institution of Communications (CIC), a Radio Application and Management Technical Committee Member of CIC, a Senior Member of China Computer Federation (CCF), a Sensor Network Technical Committee Member of CCF, an H Subcommittee Member of China Radio Interference Standard Technology Committee, the General Secretary of China UWB Forum, and the General Secretary of China Bluetooth Forum.

**Arumugam Nallanathan** (S'97–M'00–SM'05) is currently a Professor of wireless communications with the Department of Informatics, King's College London (University of London), London, U.K. He served as the Head of Graduate Studies with the School of Natural and Mathematical Sciences, King's College London, in 2011–2012. He was an Assistant Professor with the Department of Electrical and Computer Engineering, National University of Singapore, from August 2000 to December 2007. His research interests include 5G technologies, millimeter-wave communications, cognitive radio, and relay networks. In these areas, he coauthored nearly 250 papers.

Prof. Nallanathan currently serves as the Chair for the Signal Processing and Communication Electronics Technical Committee of the IEEE Communications Society. He served as the Technical Program Cochair (MAC track) for the IEEE WCNC 2014 and the IEEE International Conference on UWB 2011 (IEEE ICUWB 2011); a Cochair for the IEEE GLOBECOM 2013 (Communications Theory Symposium), the IEEE ICC 2012 (Signal Processing for Communications Symposium), the IEEE GLOBECOM 2011 (Signal Processing for Communications Symposium), the IEEE ICC 2009 (Wireless Communications Symposium), and the IEEE GLOBECOM 2008 (Signal Processing for Communications Symposium); and the General Track Chair for the IEEE VTC 2008. He is a Distinguished Lecturer of the IEEE Vehicular Technology Society. He is an Editor of the IEEE TRANSACTIONS ON COMMUNICATIONS and the IEEE TRANSACTIONS ON VEHICULAR TECHNOLOGY. He was an Editor of the IEEE TRANSACTIONS ON WIRELESS COMMUNICATIONS (2006–2011), the IEEE WIRELESS COMMUNICATIONS LETTERS, and the IEEE SIGNAL PROCESSING LETTERS. He is a corecipient of the Best Paper Award presented at the 2007 IEEE International Conference on Ultra-Wideband (ICUWB'2007). He received the IEEE Communications Society SPCE Outstanding Service Award 2012 and IEEE Communications Society RCC Outstanding Service Award 2014.